

Spin-orbit torque generated by amorphous $\text{Fe}_x\text{Si}_{1-x}$

Cheng-Hsiang Hsu^{1*}, Julie Karel^{2,3*}, Niklas Roschewsky⁴, Suraj Cheema⁵, Dinah Simone Bouma^{4,6},
Shehrin Sayed¹, Frances Hellman^{4,5,6}, Sayeef Salahuddin^{1,6}

¹*Department of Electrical Engineering and Computer Science, University of California, Berkeley, California 94720, USA*

²*Department of Materials Science and Engineering, Monash University, Clayton, Victoria 3800, Australia*

³*Australian Research Council Centre of Excellence in Future Low-Energy Electronics Technologies, Monash University, Clayton, Victoria 3800, Australia*

⁴*Department of Physics, University of California, Berkeley, California 94720, USA*

⁵*Department of Materials Science and Engineering, University of California, Berkeley, California 94720, USA*

⁶*Materials Science Division, Lawrence Berkeley National Laboratory, Berkeley, California 94720, USA*

****These authors contributed equally to this work***

While tremendous work has gone into spin-orbit torque¹⁻¹⁴ and spin current generation^{15,16}, charge-to-spin conversion efficiency remains weak in silicon¹⁷ to date, generally stemming from the low spin-orbit coupling (low atomic number, Z) and lack of bulk lattice inversion symmetry breaking. Here we report the observation of spin-orbit torque in an amorphous, non-ferromagnetic $\text{Fe}_x\text{Si}_{1-x}$ / cobalt bilayer at room temperature, using spin torque ferromagnetic resonance^{1,3,4,7-9,11,12} and harmonic Hall measurements^{5,6,10,18,19}. Both techniques provide a minimum spin torque efficiency of about 3 %, comparable to prototypical heavy metals such as Pt¹ or Ta³. According to the conventional theory of the spin Hall effect^{3,20,21}, a spin current in an amorphous material is not expected to have any substantial contribution from the electronic bandstructure. This, combined with the fact that $\text{Fe}_x\text{Si}_{1-x}$ does not contain any high- Z element, paves a new avenue for understanding the underlying physics of spin-orbit interaction and opens up a new class of material systems - silicides - that is directly compatible with complementary metal-oxide-semiconductor (CMOS) processes²²⁻²⁴ for integrated spintronics applications.

Spin-orbit torque (SOT) induced magnetization switching has shown great potential for next-generation magnetic memory technologies²⁵. Intense effort is currently in place to explore new materials for and new mechanisms of SOT as well as its use for next generation logic computing and beyond¹⁴⁻¹⁶. Conventionally, when an in-plane current is applied through the non-magnetic underlayer with strong spin-orbit interaction in a non-magnetic / magnetic heterostructure, a transverse spin current is generated. There are two main physical mechanisms responsible for the spin current: (i) spin Hall effect (SHE) stemming from Berry curvature of the bulk bandstructure or scattering off heavy (large atomic number, Z) impurities^{1,20,21,26} and (ii) the Rashba-Edelstein effect (REE) due to broken inversion symmetry at the interface^{2,27,28}. The spin current in turn exerts a torque on an adjacent magnetic layer²⁹⁻³¹. In most material systems, these two physical mechanisms can act in parallel, and it has been challenging to differentiate their separate contributions quantitatively¹³.

Spin-orbit torque has been demonstrated in various non-magnetic materials including heavy metals¹⁻³, topological insulators^{4,7}, semiconductors^{8,9}, two dimensional materials^{10,11}, and three dimensional semi-metals¹². Beyond these prototypical materials, here we report the observation of spin-orbit torque in an amorphous, non-ferromagnetic iron silicide ($a\text{-Fe}_x\text{Si}_{1-x}$) and cobalt (Co) bi-layer at room temperature. By injecting an in-plane charge current in $a\text{-Fe}_x\text{Si}_{1-x}$, a torque is exerted on the magnetic moments in the adjacent cobalt layer (Fig. 1a). This torque results in an appreciable modulation of the magnetization that is detected electrically via the spin torque ferromagnetic resonance technique and harmonic Hall measurement. Both techniques yield a minimum spin torque efficiency of approximately 3 %, which is the same order of magnitude as platinum (8

$\%$)¹ and 300 times larger than the spin Hall angle (spin torque efficiency) reported in crystalline, p-type silicon (0.01 $\%$)¹⁷. In contrast to the trends observed conventionally, substantial spin orbit torque from an amorphous, low-Z material indicates that a reasonably strong spin current can be generated in a material lacking a bandstructure or heavy element.

$\text{Fe}_x\text{Si}_{1-x}$, along with many other transition metal silicides, has been utilized extensively in the semiconductor industry. For decades, silicides have been instrumental in forming electrical contacts, gate electrodes, local interconnects and diffusion barriers²³ in very large scale integration (VLSI) technologies. Moreover, self-aligned silicidation (SALICIDE) remains a critical process in ensuring low contact and series resistance to the source and drain region of a planar metal-oxide-semiconductor field-effect transistor (MOSFET)^{22,24}. Metal silicides remain a crucial technology as the down scaling of transistors progresses, enabling better performance and denser packing of devices on an integrated circuit. In our $\text{Fe}_x\text{Si}_{1-x}$ films, the silicon composition ranges between 55 $\%$ and 60 $\%$. The amorphous nature of $\text{Fe}_x\text{Si}_{1-x}$ films with similar concentration has been studied extensively^{32,33}, and the amorphous structure in our devices was further confirmed by high-resolution cross-sectional transmission electron microscopy (HR-TEM) and synchrotron grazing incidence X-ray diffraction performed directly on the bi-layers. In the HR-TEM image (Fig. 1b), no nanocrystal formation or evidence of lattice fringes are observed across the $\text{Fe}_x\text{Si}_{1-x}$ layer. Additional TEM based structural characterizations of $\text{Fe}_x\text{Si}_{1-x}$ such as local fast Fourier transform also confirm its amorphous phase (Extended Data Fig. 1). In Fig. 1c, the X-ray 2D pole figure shows the diffraction pattern of a 10 nm $\text{Fe}_{45}\text{Si}_{55}$ film. A highly diffused pattern is observed and only sharp peaks and Kikuchi lines corresponding to the single crystal silicon substrate are present.

By contrast, the $\text{Fe}_{45}\text{Si}_{55}$ / Co bilayer contains additional reflections from the thin crystalline cobalt layer (Fig. 1d). The absence of a diffraction signal from the silicide layer confirms the lack of long-range order or nanocrystals in the $\text{Fe}_x\text{Si}_{1-x}$ thin films (Extended Data Fig. 2).

Our bilayers constitute approximately 6 to 10 nm of a- $\text{Fe}_x\text{Si}_{1-x}$ and 4 nm of cobalt, grown on amorphous silicon nitride on silicon substrates with oxidized aluminum as a capping layer to prevent the cobalt surface from oxidizing (Fig. 1a). a- $\text{Fe}_x\text{Si}_{1-x}$ and cobalt are grown by electron beam evaporation with controlled composition of iron and silicon via co-evaporation; compositions were verified using Rutherford Backscattering Spectrometry. Aluminum, which is subsequently oxidized by exposure to air, is deposited from an effusion cell. The cobalt magnetic moments are oriented in-plane (Extended Data Fig. 3), and the a- $\text{Fe}_x\text{Si}_{1-x}$ layer at both compositions ($x=40$ and 45 %) show no appreciable ferromagnetism (Extended Data Fig. 4). For device fabrication, we use Ar ion-milling and optical lithography to pattern the film stack into desired device structures.

To characterize the SOT in a- $\text{Fe}_x\text{Si}_{1-x}$ / Co, we first performed harmonic Hall measurements of the effective magnetic fields due to SOT^{5,6,10,18,19}. The samples are patterned into a single Hall bar structure (Fig. 2b) and an a.c. current is injected along the x-axis (Fig. 2a). Both first ($V_{1\omega}$) and second ($V_{2\omega}$) harmonic transverse voltages are detected (Fig. 2c, d). During the measurement, the equilibrium direction of the Co magnetic moments is pinned by a fixed in-plane external magnetic field as the sample is rotated. We conduct this in-plane angle scan as a function of both current and magnetic field magnitude. If a SOT is present, a quasi-static oscillation of the cobalt moments can be induced and hence an oscillating Hall voltage. In this case, a Hall voltage at twice the injected

a.c. current frequency will be excited^{5,6} (Fig. 2d). In addition to the SOT contribution, $V_{2\omega}$ also includes signals induced from the thermoelectric effects due to joule heating of the oscillating current that scales quadratically with current. Thus, thermal effects such as ordinary Nernst effect (ONE) and anomalous Nernst effect (ANE) can be present in $V_{2\omega}$ and extracting the SOT effect requires careful analysis¹⁹ (see also Methods, Extended Data Fig. 5).

After doing the comprehensive angle (φ_B), current and magnetic field dependent sweeps, we carefully analyzed $V_{2\omega}$. First, the coefficient of the $\cos(2\varphi_B)\cos(\varphi_B)$ component is extracted, giving the field (FL) -like torque effective field voltage that scales as $1/B_{ext}$ (Extended Data Fig. 5b). The FL-like torque effective field includes both the FL-like spin-orbit torque ($\Delta B_{FL,SOT}$) and FL-like torque due to Oersted field (B_{Oe}) contribution. By filtering out the Oersted field, strong FL-like SOT effective fields are still present (Fig. 2e). Next, we are left with a $\cos(\varphi_B)$ term which contains three contributions including the damping (DL) -like torque effective field (ΔB_{DL}), ANE and ONE (Extended Data Fig. 5a). By considering the magnetic field dependent sweep, we can distinguish between these three contributions separately since the DL-like torque effective field scales as $1/(B_{ext} + \mu_0 M_{eff})$ (Extended Data Fig. 5c), the ANE is constant with external field and the ONE scales linearly with external field¹⁹. In our data, clear signatures of both the DL-like and FL-like effective fields due to spin-orbit torque are present (Fig. 2e, f). Both the field-like and damping-like effective fields scale linearly with the injected current densities in the $\text{Fe}_x\text{Si}_{1-x}$ layer, confirming the presence of both DL-like and FL-like SOTs (Fig. 2e, f).

We further confirmed and characterized spin-torque strength by spin-torque ferromagnetic

resonance (ST-FMR) which, in the past, has been used to quantify SOT strength in heavy metals, topological insulators and semi-metals^{1,3,4,7-9,11,12}. The schematic of the measurement setup is shown in Fig. 3a. We fabricated 3 x 9 micron strips and contacted them with co-planar waveguides (Fig. 3b) for radio-frequency (RF) current injection. The injected in-plane RF microwave current induces a torque that acts on the magnetization of the Co layer, yielding an oscillating anisotropic magnetoresistance (AMR). By sweeping an in-plane field, the criteria of ferromagnetic resonance can be fulfilled and a resonance line shape can be obtained by measuring the d.c. mix down voltage (V_{mix}) stemming from the mixing between the oscillating AMR and RF current. From the line shape of V_{mix} versus external field, symmetric and anti-symmetric components are extracted which respectively correspond to the in-plane ($\hat{m} \times (-\hat{y} \times \hat{m}), \parallel$) and out-of-plane ($-\hat{y} \times \hat{m}, \perp$) component of the current-induced torques (Fig. 3a).

The resulting (V_{mix}) line shapes measured at frequencies from 6.5 GHz to 9 GHz shows a strong presence of resonance due to the SOT in the a-Fe₄₅Si₅₅ (8) / Co (4) bilayer (Fig. 3c). The magnetic field is oriented in-plane with angle of $\varphi_B = 45^\circ$ from the current direction. To analyze the details of various components of the SOT, we fitted both a symmetric and an antisymmetric Lorentzian function (Methods) to the line shape. A typical fit is shown at 6.5 GHz in Fig. 3d. Both symmetric and anti-symmetric components are clearly present.

The often-used figure of merit for charge-to-spin conversion efficiency is the so-called spin torque efficiency ξ . Notably, this metric captures all possible spin current generation mechanisms and is not only limited to the bulk spin Hall effect. The harmonic Hall measurement and the

ST-FMR measurement separately and independently provide a measure of ξ . From the harmonic Hall measurement, assuming perfect interface transparency, i.e, the magnet absorbs all generated spins or all transferred momentum, the effective spin torque efficiency follows^{6,18} $\xi_{DL} = 2 | e | M_s t_{FM} \mu_0 H_{DL} / (\hbar j_{NM})$, where M_s is the saturation magnetization of Co (Extended Data Fig. 3), t_{FM} is the thickness of Co, $\mu_0 H_{DL}$ is the damping-like torque effective field strength and j_{NM} is the current density flowing through the $\text{Fe}_x\text{Si}_{1-x}$ layer (Methods). Notably, this expression captures the amount of spin current generated per charge current injected in the $\text{Fe}_x\text{Si}_{1-x}$ layer. From the analysis, we obtained a ξ_{DL} of 11.92 % for a- $\text{Fe}_{40}\text{Si}_{60}$ / Co and 3.98 % for a- $\text{Fe}_{45}\text{Si}_{55}$ / Co (Table 1).

From the ST-FMR technique, the ξ_{DL} can be calculated from the expression¹ $\xi_{DL} = (S/A) (| e | \mu_0 M_s t_{FM} t_{NM} / \hbar) \sqrt{1 + (4\pi M_{eff} / H_{res})^2}$, where S/A is the ratio between the symmetric (V_s) and antisymmetric (V_A) Lorentzian of V_{mix} , μ_0 is the vacuum permeability, t_{NM} is the thickness of the a- $\text{Fe}_x\text{Si}_{1-x}$, H_{res} is the resonance field and $4\pi M_{eff}$ is the demagnetization field obtained by fitting to the Kittel relation (Extended Data Fig. 6). This method assumes that the V_A is dominantly attributed to the FL-like torque due to Oersted field which under the presence of strong FL-like SOT may obscure the accuracy of the ξ_{DL} . Since the FL-like SOT effective field and Oersted field are confirmed to be in the same direction from the harmonic Hall measurement, this method actually serves as a lower bound of ξ_{DL} . Historically, it has also been shown that different methods of ξ_{DL} extraction with ST-FMR yielded values less than one order of magnitude difference⁷. The accurate ξ_{DL} could vary between techniques, nevertheless, the ST-FMR serves the main purpose to confirm the presence of SOT in $\text{Fe}_x\text{Si}_{1-x}$ / Co. From the analysis, we obtained a ξ_{DL} of 4.30

% for a-Fe₄₀Si₆₀ / Co and 2.56 % for a-Fe₄₅Si₅₅ / Co (Table 1). Finally, to probe the effect of Fe in the a-Fe_xSi_{1-x} layer with respect to the SOT, a control experiment was performed using heavily phosphorous-doped amorphous silicon with no iron doping. No discernible spin-orbit torque signature could be found in either the ST-FMR (Extended Data Fig. 7) or in the harmonic Hall measurements (Extended Data Fig. 8). Therefore, the presence of Fe is clearly necessary for spin current generation in a-Fe_xSi_{1-x}.

Recent work has shown that an intrinsic contribution to spin current is possible from the anomalous Hall effect^{34,35}. However, this not only requires a fixed ferromagnet as spin source but also utilizes ferromagnet-spacer-ferromagnet structure^{36,37} and the torque follows the symmetry of a spin accumulation in the magnetization direction of the fixed ferromagnet. Both device configuration and torque symmetry are completely different from our experiments (see Methods for more details). On the other hand, the torque symmetry observed in our experiments are well aligned with what would be expected from a giant SHE and/or Rashba-like interfacial torque. However, the conventional theory describing the intrinsic contribution to the SHE cannot be directly applied as it is formulated based on crystal momentum, \mathbf{k} , which is no longer a good quantum number in amorphous materials due to the absence of lattice periodicity. This point, together with the fact that neither of the elements, Fe or Si, are heavy, make this work very distinct from existing reports on spin orbit torque and spin current generation. Historically, it has been very challenging to cleanly separate out effects owing to the broken symmetry at the interface from those coming from bulk bandstructure of the SOT metal. By contrast, in our experiments any effect coming from the bulk bandstructure is expected to be minimal.

To summarize, we have demonstrated that amorphous $\text{Fe}_x\text{Si}_{1-x}$ can generate a SOT of similar magnitude as prototypical heavy metals such as Ta³ or Pt¹. The observed SOT does not conform directly to the conventional theories of spin current generation¹³, indicating a potentially new mechanism for spin-orbit torque. This work also extends spin current generation to a completely new class of materials, i.e. silicides, which is ubiquitously used in CMOS technology. The diverse set of available silicides provides an exciting playground for investigating the underlying physics of spin current generation as well as potential for use in integrated Si technology.

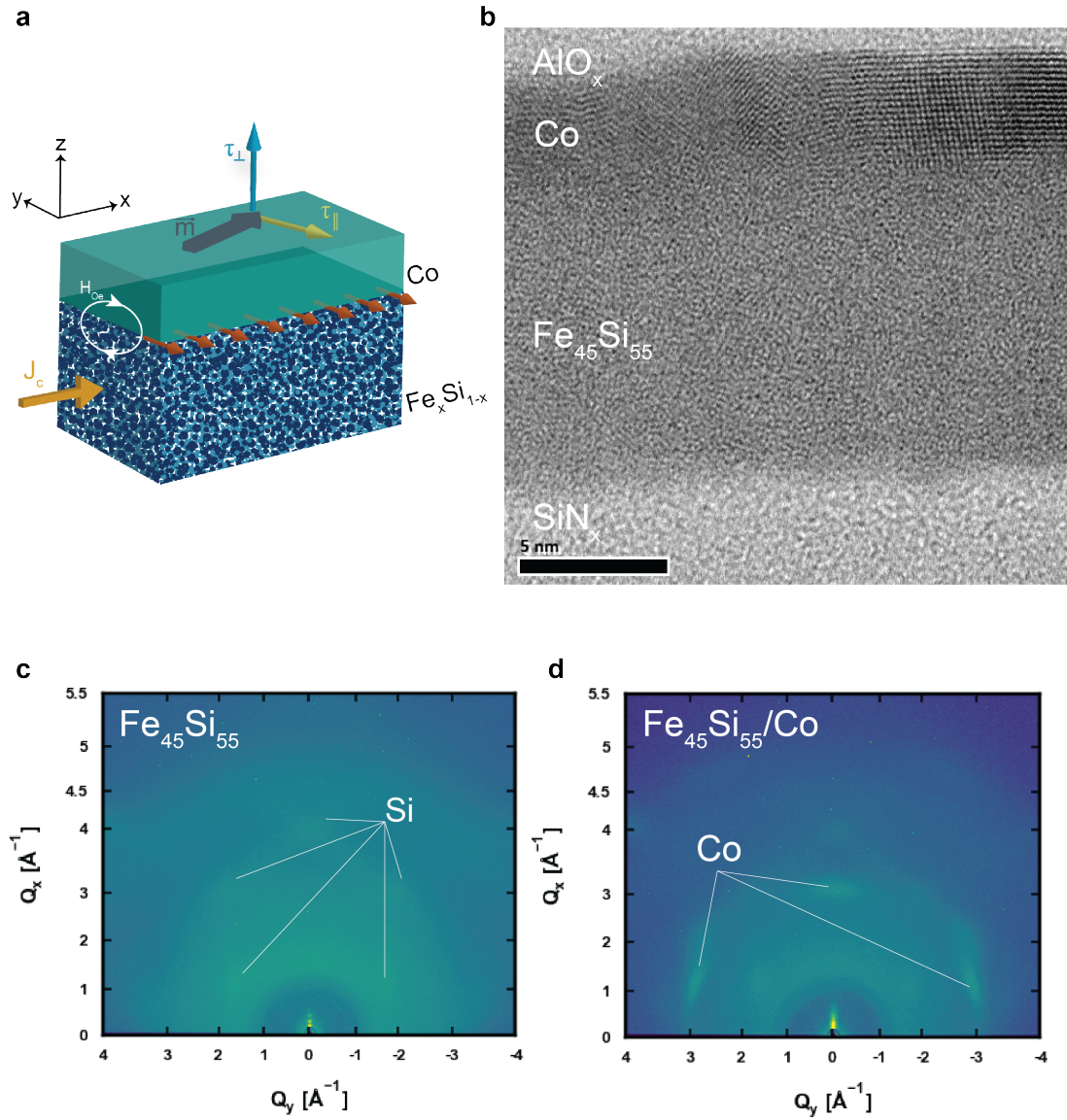


Fig. 1. Structural characterization of the $\text{Fe}_x\text{Si}_{1-x}$ / cobalt bilayer with high-resolution transmission electron microscopy and synchrotron X-ray diffraction. (a) Details of the sample stacks under study. (b) High-resolution cross-sectional TEM of the sample with $\text{Fe}_x\text{Si}_{1-x}$ ($x=45\%$). The $\text{Fe}_x\text{Si}_{1-x}$ layer shows a fully amorphous structure without any nanocrystal forma-

tion. The $\text{Fe}_x\text{Si}_{1-x}$ layer is grown on a 300 nm amorphous silicon nitride on silicon substrate. The cobalt layer is capped with 2 nm oxidized aluminum then 3 nm of silicon nitride (partially shown as the topmost layer). **(c)** Synchrotron X-ray two-dimensional pole figure of bare $\text{Fe}_{45}\text{Si}_{55}$ (10 nm) on a 300 nm silicon nitride on silicon substrate capped with 2 nm aluminum oxide. Only concentrated intensities corresponding to silicon (1 1 1) and (2 2 0) forming the Kikuchi lines are present. Otherwise, diffuse patterns from the amorphous $\text{Fe}_x\text{Si}_{1-x}$ show the lack of long-range order. **(d)** Synchrotron X-ray two-dimensional pole figure of $\text{Fe}_{45}\text{Si}_{55}$ (8 nm) / Co (4 nm) on 300 nm silicon nitride on silicon substrate capped with 2 nm aluminum oxide. On top of the silicon (1 1 1) and (2 2 0) peaks, additional sharp cobalt peaks are the only contrast to the $\text{Fe}_{45}\text{Si}_{55}$ bare film 2D pole figure.

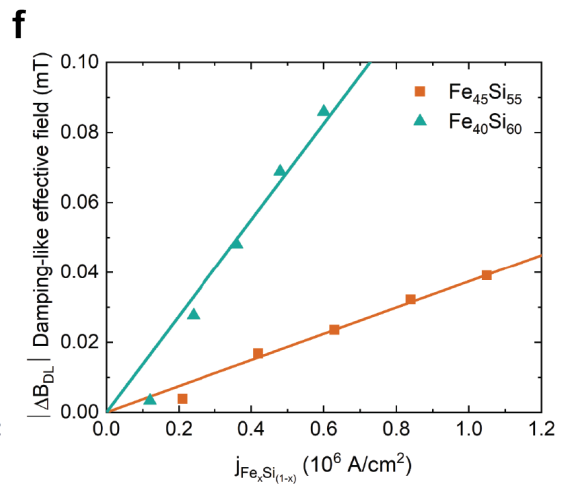
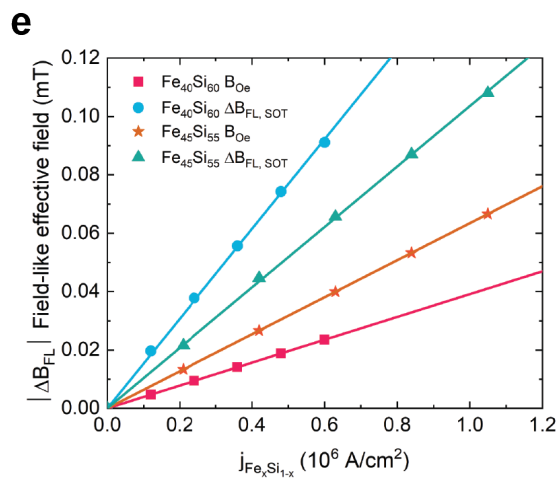
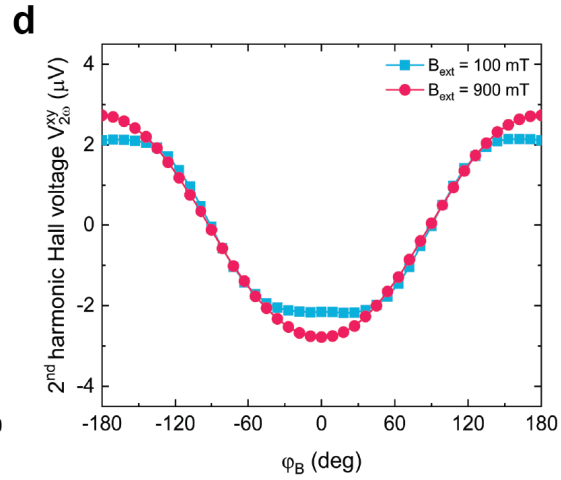
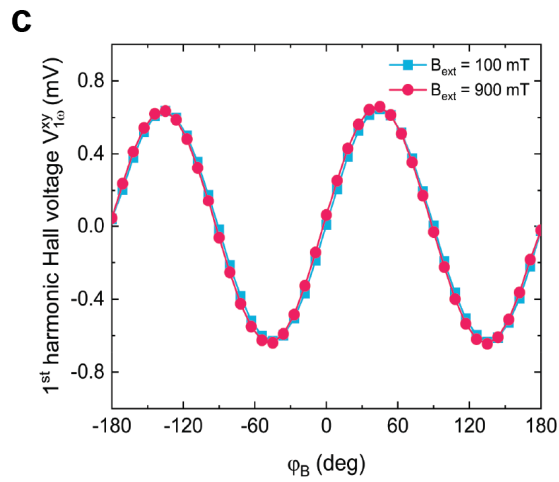
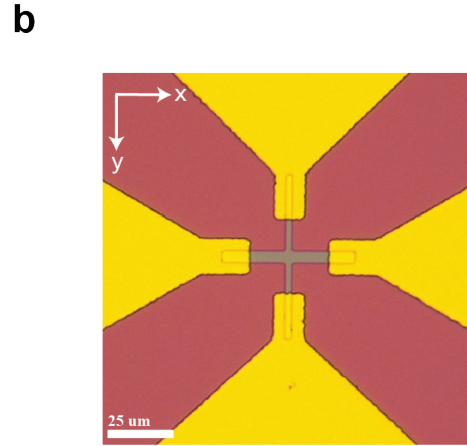
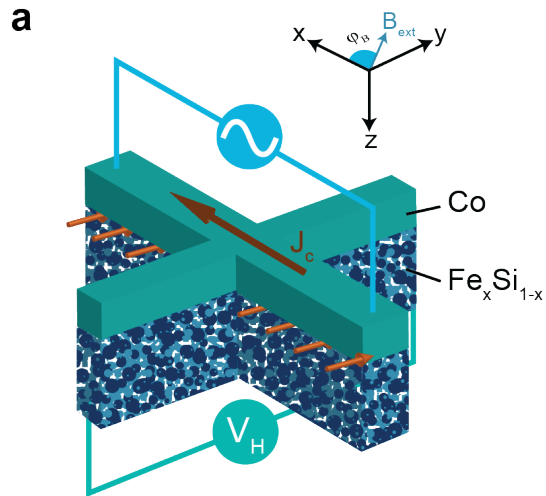


Fig. 2. Harmonic Hall measurement of $\text{Fe}_x\text{Si}_{1-x}$ / cobalt bilayer. (a) Schematic of the harmonic Hall measurement setup. Low frequency a.c. current is applied along the x-direction and the magnetic moments of cobalt are pinned by a rotating external magnetic field in the xy plane. (b) Optical microscope image of the fabricated single Hall bar device. The current line is 5 micron in width and the voltage line is 3 micron in width. Both lines are 30 micron in length. (c) First harmonic voltage of the $\text{Fe}_{45}\text{Si}_{55}$ / cobalt bilayer. The first harmonic voltage is essentially the planar Hall voltage that scales as $\sin(2\varphi_B)$. (d) Second harmonic voltage of the $\text{Fe}_{45}\text{Si}_{55}$ / cobalt bilayer. The second harmonic voltage contains information on field-like (FL) torque effective field, damping-like (DL) torque effective field and thermoelectric effects. The FL-like torque effective field scales as $\cos(2\varphi_B)\cos(\varphi_B)$. The DL-like torque effective field and thermoelectric effect scale as $\cos(\varphi_B)$. (e) FL-like torque effective field due to SOT and Oersted field as a function of injected current density in the $\text{Fe}_x\text{Si}_{1-x}$ layer. The linear trend confirms the presence of appreciable FL-like spin-orbit torque. (f) DL-like torque effective field as a function of injected current density in the $\text{Fe}_x\text{Si}_{1-x}$ layer. The linear trend confirms the presence of appreciable DL-like spin-orbit torque.

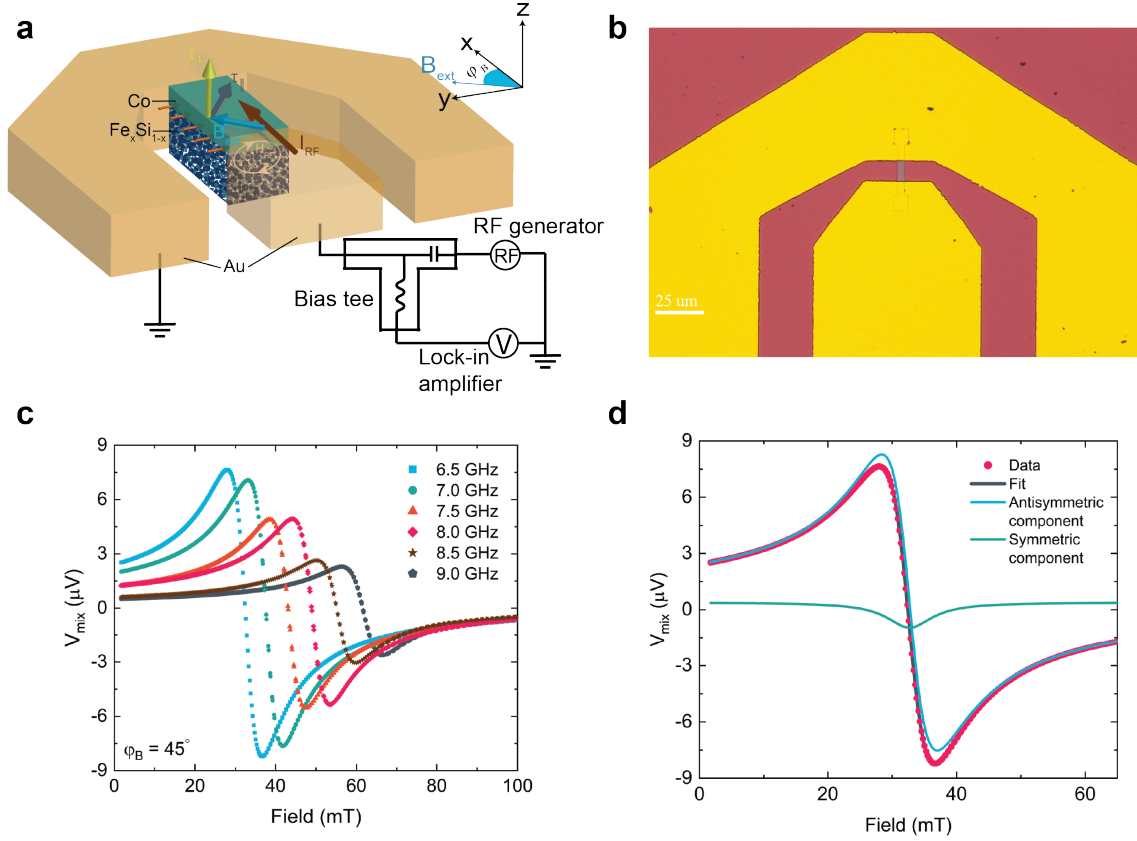


Fig. 3. Spin-torque ferromagnetic resonance (ST-FMR) measurement of $\text{Fe}_{45}\text{Si}_{55}$ (8) / cobalt (4) bilayer. (a) Schematic of the ST-FMR setup and sample geometry under study. τ_{\parallel} is the in-plane current-induced torque component, τ_{\perp} is the out-of-plane current-induced torque component and φ_B is the angle spanned between the in-plane field and RF current direction. (b) Optical microscope image of fabricated ST-FMR device with dimension of 3 micron in width and 9 micron in length. The coplanar waveguide (gold color) serves as the microwave transmission contact to the device. (c) ST-FMR spectrum measured on $\text{Fe}_{45}\text{Si}_{55}$ (8) / cobalt (4) versus applied external magnetic field with RF frequency from 6.5 GHz to 9 GHz. (d) ST-FMR V_{mix} lineshape fitting on $\text{Fe}_{45}\text{Si}_{55}$ (8) / cobalt (4) versus external magnetic field at RF frequency 6.5 GHz (Methods).

Sample	Harmonic Hall	ST-FMR
$\text{Fe}_{40}\text{Si}_{60} / \text{Co}$	11.92 %	4.30 %
$\text{Fe}_{45}\text{Si}_{55} / \text{Co}$	3.98 %	2.56 %

Table 1. Spin torque efficiency $|\xi_{DL}|$ extracted from harmonic Hall measurement and ST-FMR on $\text{Fe}_x\text{Si}_{1-x} / \text{cobalt bilayer}$.

1. Liu, L., Moriyama, T., Ralph, D. C. & Buhrman, R. A. Spin-torque ferromagnetic resonance induced by the spin hall effect. *Physical Review Letters* **106**, 036601 (2011).
2. Miron, I. M. *et al.* Perpendicular switching of a single ferromagnetic layer induced by in-plane current injection. *Nature* **476**, 189–193 (2011).
3. Liu, L. *et al.* Spin-torque switching with the giant spin hall effect of tantalum. *Science* **336**, 555–558 (2012).
4. Mellnik, A. R. *et al.* Spin-transfer torque generated by a topological insulator. *Nature* **511**, 449–451 (2014).
5. Hayashi, M., Kim, J., Yamanouchi, M. & Ohno, H. Quantitative characterization of the spin-orbit torque using harmonic hall voltage measurements. *Physical Review B* **89**, 144425 (2014).
6. Avci, C. O. *et al.* Interplay of spin-orbit torque and thermoelectric effects in ferromagnet/normal-metal bilayers. *Physical Review B* **90**, 224427 (2014).
7. Wang, Y. *et al.* Topological surface states originated spin-orbit torques in Bi_2Se_3 . *Physical Review Letters* **114**, 257202 (2015).
8. Chen, L. *et al.* Robust spin-orbit torque and spin-galvanic effect at the Fe/GaAs (001) interface at room temperature. *Nature Communications* **7**, 13802 (2016).
9. Skinner, T. D. *et al.* Complementary spin-hall and inverse spin-galvanic effect torques in a ferromagnet/semiconductor bilayer. *Nature Communications* **6**, 6730 (2015).

10. Shao, Q. *et al.* Strong rashba-edelstein effect-induced spin-orbit torques in monolayer transition metal dichalcogenide/ferromagnet bilayers. *Nano Letters* **16**, 7514–7520 (2016).
11. MacNeill, D. *et al.* Control of spin-orbit torques through crystal symmetry in wte 2 /ferromagnet bilayers. *Nature Physics* **13**, 300–305 (2017).
12. Nan, T. *et al.* Anisotropic spin-orbit torque generation in epitaxial srir0 3 by symmetry design. *Proceedings of the National Academy of Sciences* **116**, 16186–16191 (2019).
13. Manchon, A. *et al.* Current-induced spin-orbit torques in ferromagnetic and antiferromagnetic systems. *Reviews of Modern Physics* **91**, 035004 (2019).
14. Luo, Z. *et al.* Current-driven magnetic domain-wall logic. *Nature* **579**, 214–218 (2020).
15. Noël, P. *et al.* Non-volatile electric control of spin–charge conversion in a SrTiO₃ Rashba system. *Nature* **580**, 483–486 (2020).
16. Tsai, H. *et al.* Electrical manipulation of a topological antiferromagnetic state. *Nature* **580**, 608–613 (2020).
17. Ando, K. & Saitoh, E. Observation of the inverse spin Hall effect in silicon. *Nature Communications* **3**, 629 (2012).
18. Roschewsky, N., Lambert, C. H. & Salahuddin, S. Spin-orbit torque switching of ultralarge-thickness ferrimagnetic GdFeCo. *Physical Review B* **96**, 1–5 (2017).
19. Roschewsky, N. *et al.* Spin-orbit torque and nernst effect in bi-sb/co heterostructures. *Physical Review B* **99**, 195103–195104 (2019).

20. Hirsch, J. E. Spin hall effect. *Phys. Rev. Lett.* **83**, 1834 (1999).
21. Sinova, J., Valenzuela, S. O., Wunderlich, J., Back, C. H. & Jungwirth, T. Spin hall effects. *Reviews of Modern Physics* **87**, 1213–1260 (2015).
22. Zhang, S.-L. & Östling, M. Metal Silicides in CMOS Technology: Past, Present, and Future Trends. *Critical Reviews in Solid State and Materials Sciences* **28**, 1–129 (2003).
23. Chen, L. J. Metal silicides: An integral part of microelectronics. *JOM* **57**, 24–30 (2005).
24. Ren, L. & Tu, K. Silicide technology for SOI devices. In *Silicide Technology for Integrated Circuits*, chap. 8, 201–228 (IET, The Institution of Engineering and Technology, Michael Faraday House, Six Hills Way, Stevenage SG1 2AY, UK, 2011).
25. Salahuddin, S., Ni, K. & Datta, S. The era of hyper-scaling in electronics. *Nature Electronics* **1**, 442–450 (2018).
26. Dyakonov, M. I. & Perel, V. I. Current-induced spin orientation of electrons in semiconductors. *Physics Letters A* **35**, 459–460 (1971).
27. Edelstein, V. M. Spin polarization of conduction electrons induced by electric current in two-dimensional asymmetric electron systems. *Solid State Communications* **73**, 233–235 (1990).
28. Hellman, F. *et al.* Interface-induced phenomena in magnetism. *Reviews of Modern Physics* **89**, 025006 (2017).
29. Slonczewski, J. C. Current-driven excitation of magnetic multilayers. *Journal of Magnetism and Magnetic Materials* **159**, L1–L7 (1996).

30. Ralph, D. C. & Stiles, M. D. Spin transfer torques. *Journal of Magnetism and Magnetic Materials* **320**, 1190–1216 (2008).
31. Manchon, A. & Zhang, S. Theory of nonequilibrium intrinsic spin torque in a single nanomagnet. *Physical Review B* **78** (2008).
32. Sharma, S. K., Geserich, H. P. & Theiner, W. A. Amorphous-to-Crystalline Transformation in Evaporated FeSi Films. *physica status solidi (a)* **32**, 467–474 (1975).
33. Karel, J. *et al.* Enhanced spin polarization of amorphous FeSi_{1-x} thin films revealed by Andreev reflection spectroscopy. *Physical Review Materials* **2**, 1–6 (2018).
34. Bianco, R., Resta, R. & Souza, I. How disorder affects the berry-phase anomalous hall conductivity: A reciprocal-space analysis. *Physical Review B* **90**, 125153 (2014).
35. Karel, J. *et al.* Scaling of the anomalous Hall effect in lower conductivity regimes. *EPL (Europhysics Letters)* **114**, 57004 (2016).
36. Bose, A. *et al.* Observation of Anomalous Spin Torque Generated by a Ferromagnet. *Physical Review Applied* **9**, 064026 (2018).
37. Gibbons, J. D., MacNeill, D., Buhrman, R. A. & Ralph, D. C. Reorientable Spin Direction for Spin Current Produced by the Anomalous Hall Effect. *Physical Review Applied* **9**, 064033 (2018).

Acknowledgements This work was primarily supported by the U.S. Department of Energy, Office of Science, Office of Basic Energy Sciences, Materials Sciences and Engineering Division, under Contract No. DE-AC02-05-CH11231 within the Non-Equilibrium Magnetism program (MSMAG). This work was also supported in part by the ASCENT center, one of the six centers within the JUMP initiative jointly supported by DARPA and SRC. In addition, support from NSF E3S center is gratefully acknowledged. This work was also supported through the Australian Research Council Centre of Excellence in Future Low Energy Electronics Technologies under CE170100039 and the Australian Research Council Discovery Project DP200102477. We acknowledge access to NCRIS facilities (ANFF and the Heavy Ion Accelerator Capability) at the Australian National University. Use of the Stanford Synchrotron Radiation Lightsource, SLAC National Accelerator Laboratory, is supported by the U.S. Department of Energy, Office of Science, Office of Basic Energy Sciences under Contract No. DE-AC02-76SF00515. This work was performed in part at the Berkeley Marvell Nanofabrication Laboratory at University of California, Berkeley and their staff research support is greatly appreciated.

Correspondence Correspondence and requests for materials should be addressed to C.-H.H. (chhsu@berkeley.edu) or S.S. (sayeef@berkeley.edu).